CLIC Physics Potential

James Wells & Gian Giudice

Manchester, 18 October 2011

Organization

Introductory Comments

Topic sub-editors:

Higgs Physics: Abdelhak Djouadi, Markus Schumacher

Supersymmetry: Sabine Kraml, Werner Porod

Alternative Scenarios: Roberto Contino, Christophe Grojean

Precision: Andre Hoang, Klaus Moenig

Overall sub-editor: Dan Feldman

Physics case built on bring together many different elements into this one document:
- Past CLIC study results
- Current benchmark studies
- Latest theory views consistent with all data
- Theory analyses suggesting viable search strategies and results

Gian and I wanted it to be as "picture driven" as we can, and that is how I will deliver this review report

1.2 Higgs Physics

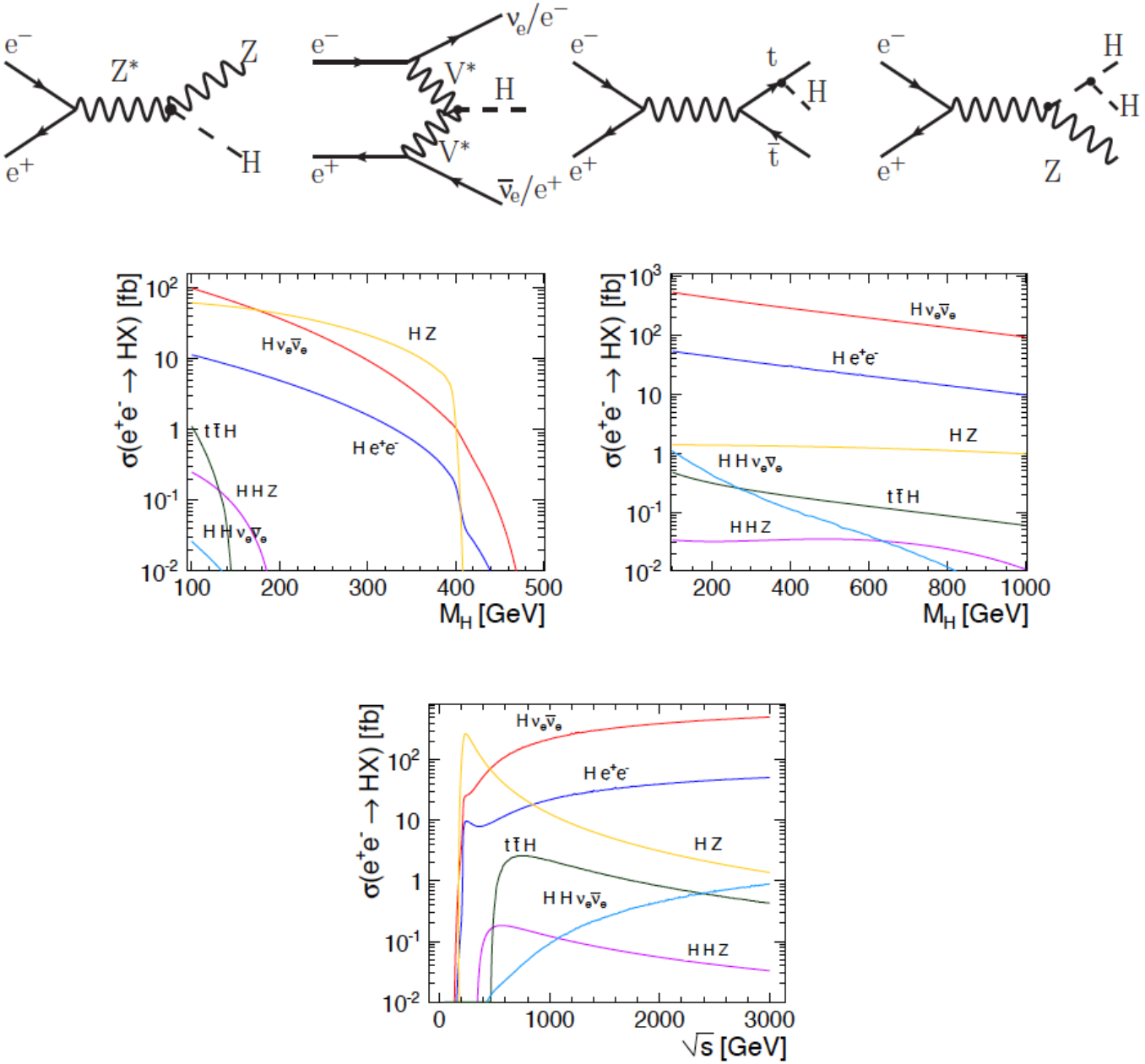

Fig. 1.1: Production mechanisms of the SM Higgs boson at CLIC (top); the total cross sections as a function of M_{H} for $\sqrt{s} = 0.5$ (middle-left), and 3 TeV (middle-right), and cross sections as a function of $\sqrt{s}$ for $M_{\mathrm{H}} = 120$ GeV (bottom).

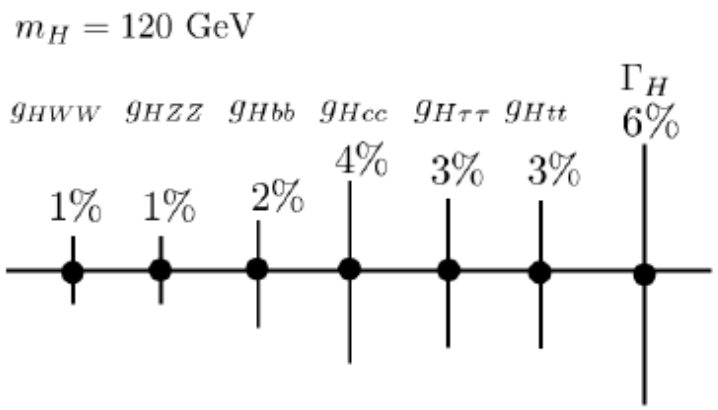

	Stat. Acc.(%)
g_{Hbb}	0.22
$g_{H\mu\mu}$	23

Fig. 1.2: Relative error in the Higgs boson coupling determination to different particle species. The top diagram is for a Higgs mass of 120 GeV at $\sqrt{s} = 500$ GeV and with 500 fb^{-1} of integrated luminosity, except $g_{t\bar{t}H}$, which is obtained at $\sqrt{s} = 800$ GeV with 1 ab^{-1}. The bottom table gives the accuracies on the couplings obtained at CLIC 3 TeV with 2 ab^{-1}, as shown in Chapter 12. These are pure statistical errors.

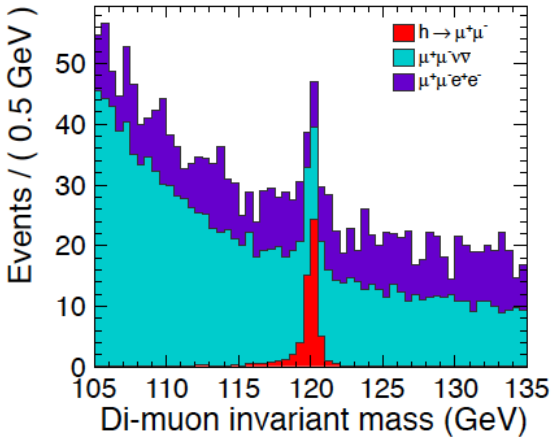

(a) $e^+e^- \to H\nu\bar{\nu}, H \to \mu^+\mu^-$

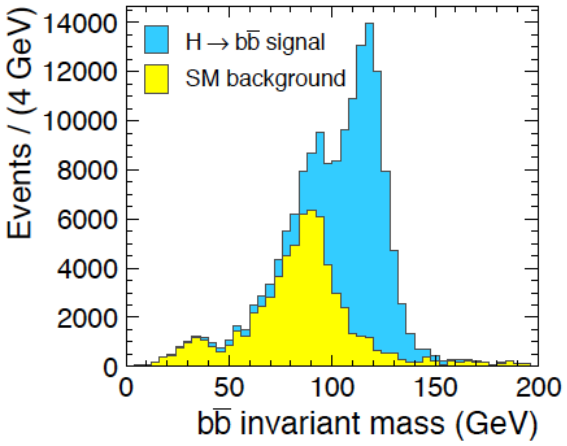

(b) $e^+e^- \to H\nu\bar{\nu}, H \to b\bar{b}$

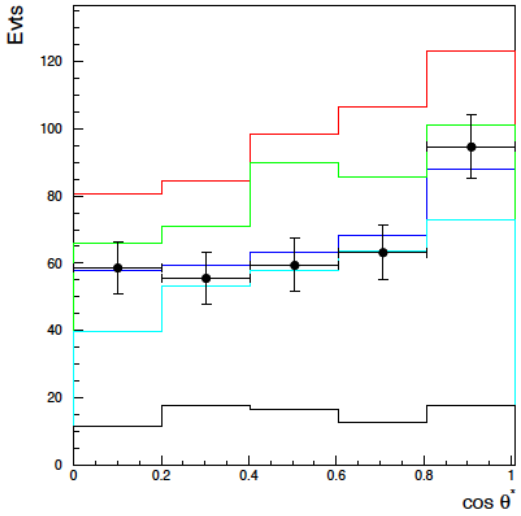

(c) $|\cos\theta^*|$ distribution

Fig. 1.3: Reconstructed sample for two Higgs channels with $M_H = 120$ GeV at CLIC with $\sqrt{s} = 3$ TeV with 2 ab^{-1} (top). The histograms are stacked distributions of signal and background reconstructed using the CLIC_SiD detector (see Chapter 12). Reconstructed $|\cos\theta^*|$ distribution for $\lambda_{HHH}/\lambda_{HHH}^{SM} = 1.25, 1.0, 0.75$ and 0.5 from bottom to top, with the points with error bars showing the expectation for 5 ab^{-1} of data [20] (bottom).

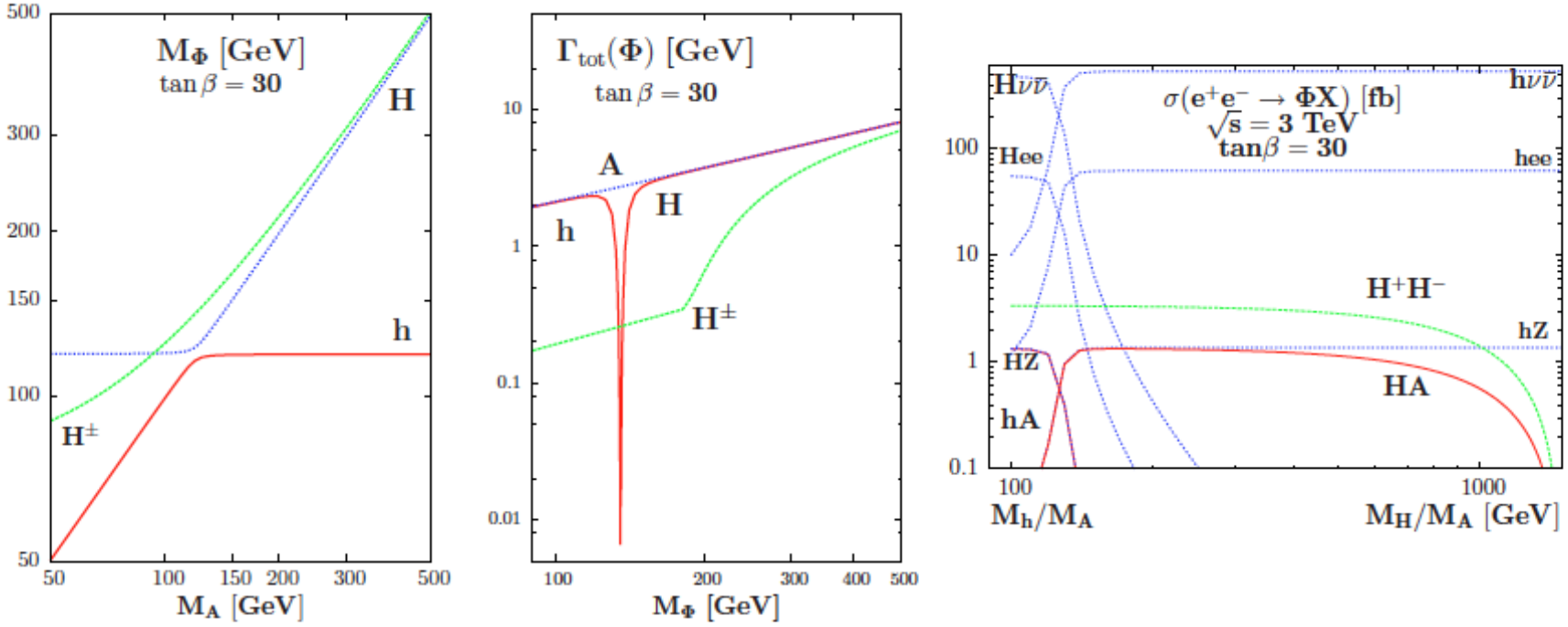

Fig. 1.4: Masses and total decay widths of the MSSM Higgs bosons for $\tan\beta = 30$ and production cross sections in e^+e^- collisions as functions of the masses in e^+e^- collisions at $\sqrt{s} = 3$ TeV; from [8].

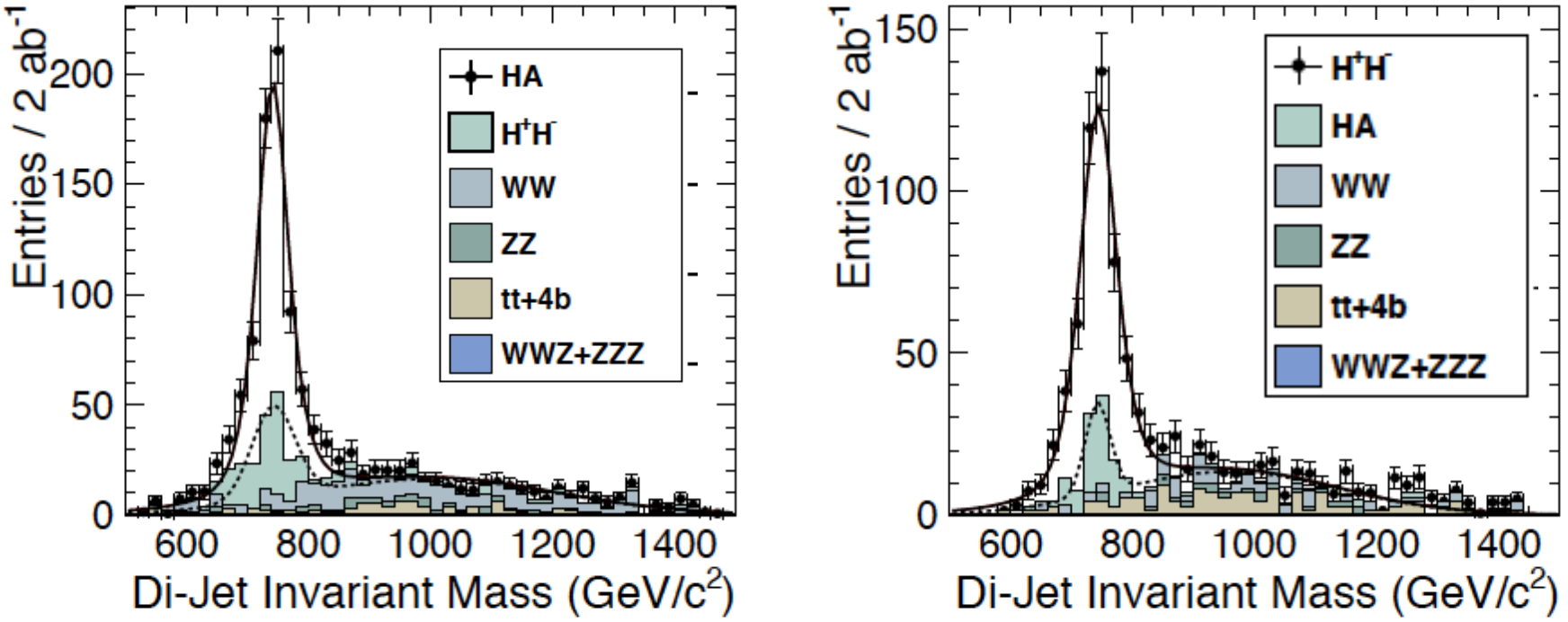

Fig. 1.5: Higgs mass peak reconstruction in the processes $e^+e^- \to HA$ (left), and in $e^+e^- \to H^+H^-$ (right), at a CLIC detector using *model II*, see Chapter 12. The corresponding background channels are shown as well. The finite Higgs widths are taken into account.

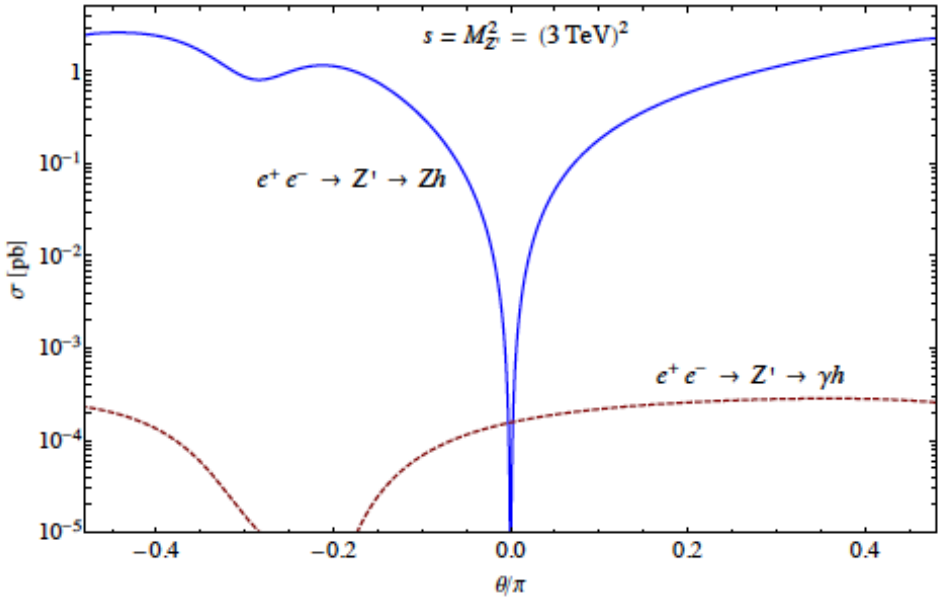

Fig. 1.6: Cross sections for the processes $e^+e^- \to Z' \to ZH$ and γH at CLIC with $\sqrt{s} = M_{Z'} = 3$ TeV as a function of a parameter that scans over minimal Z' models.

1.3 Supersymmetry

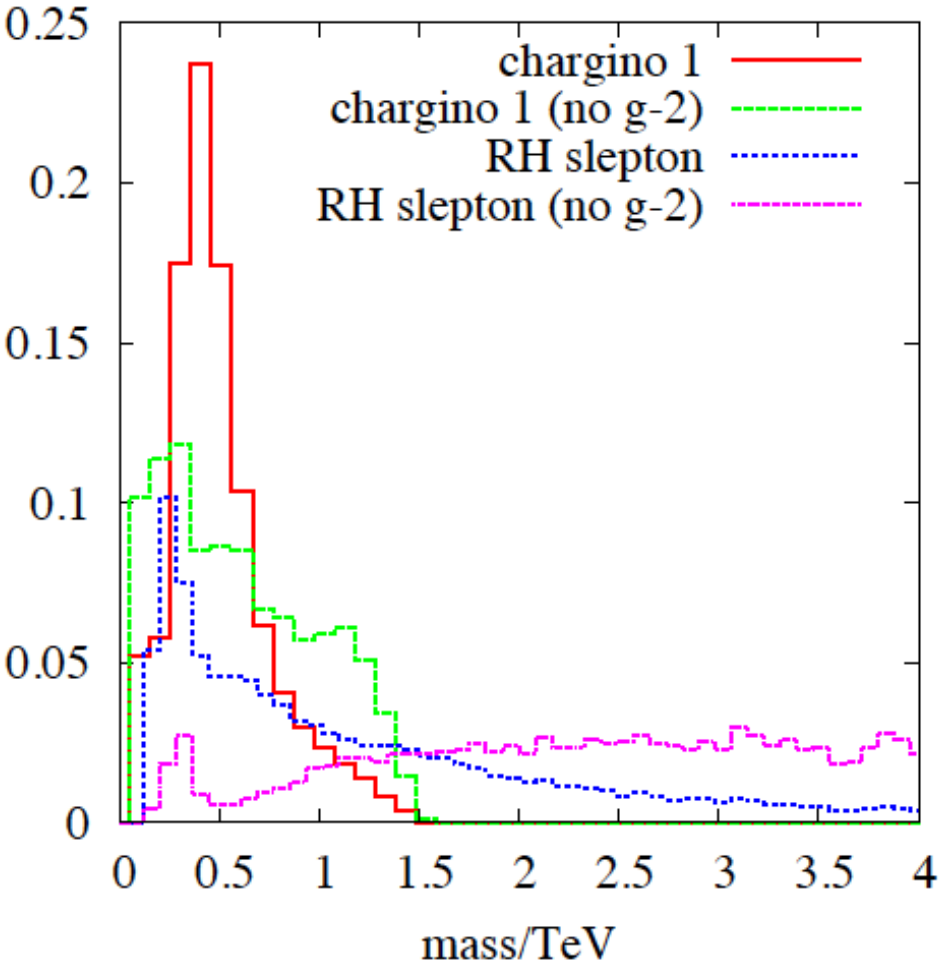

Fig. 1.7: Posterior probabilities from a global fit of the mSUGRA/CMSSM LHC searches and with flat priors in the input parameters [36].

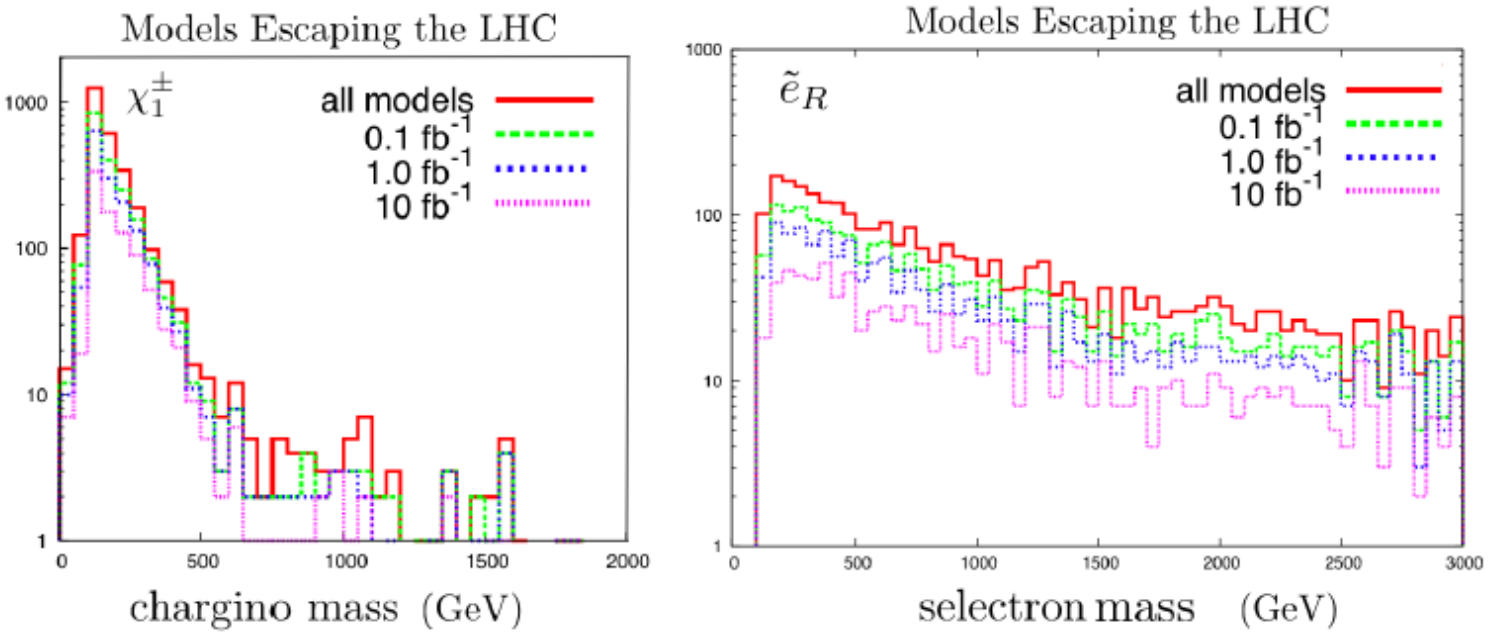

Fig. 1.8: Distribution of $\tilde{\chi}_1^\pm$ (left) and $\tilde{e}_R$ (right) masses of pMSSM points that escape 14 TeV LHC searches with 0.1 fb^{-1}, 1 fb^{-1}, and 10 fb^{-1} of integrated luminosity [41]. The top red histograms show the mass distributions in the full model set.

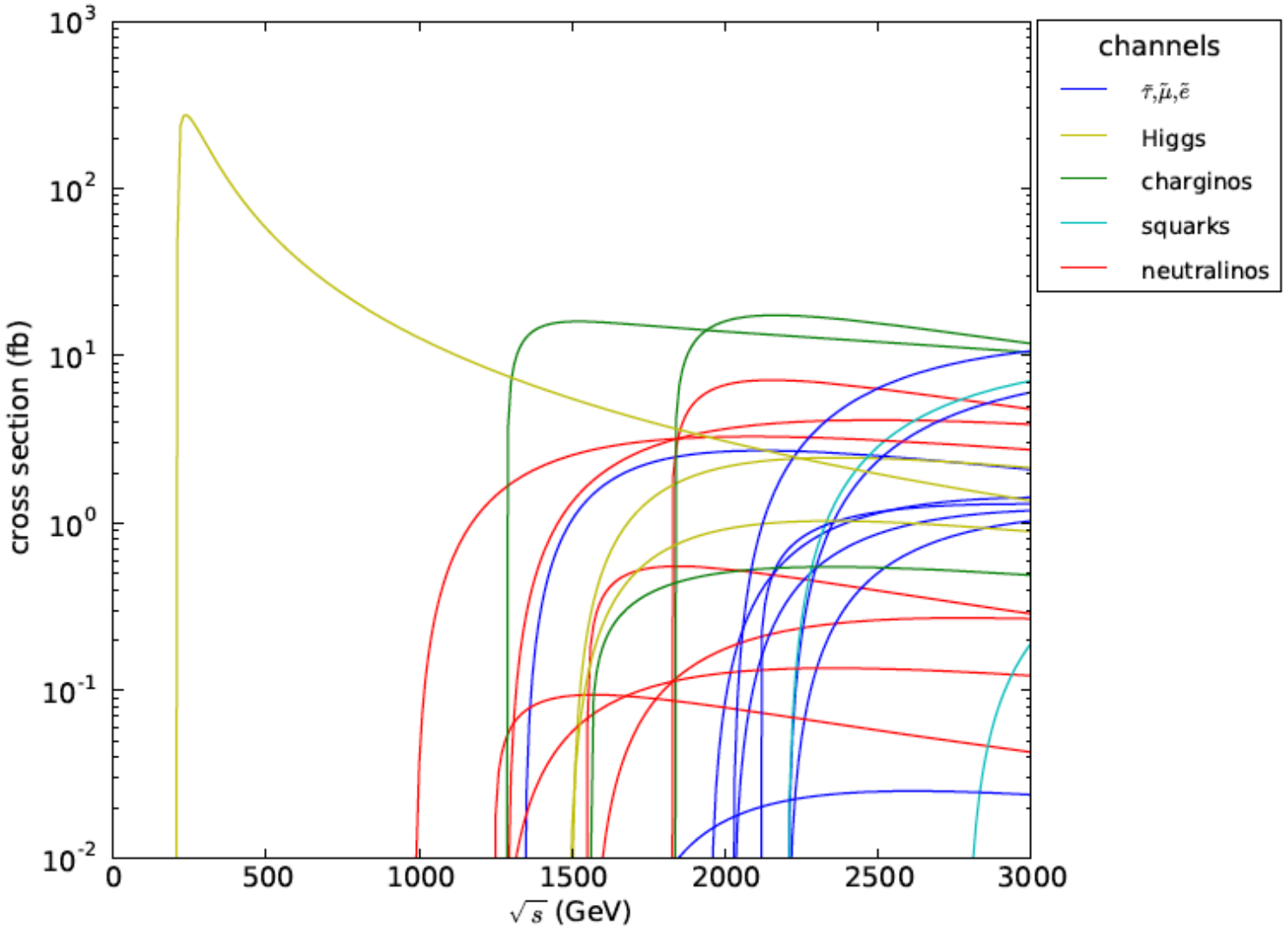

Fig. 1.9: SUSY production cross sections (in fb) of *model II* as a function of $\sqrt{s}$. Every line of a given colour corresponds to the production cross section of one of the particles in the legend, e.g. the three green lines are, per increasing threshold, $e^+e^- \to \widetilde{\chi}_1^-\widetilde{\chi}_1^+$, $e^+e^- \to \widetilde{\chi}_1^\mp\widetilde{\chi}_2^\pm$, and $e^+e^- \to \widetilde{\chi}_2^-\widetilde{\chi}_2^+$ respectively. The first threshold is the $e^+e^- \to ZH$ production.

Table 1.1: Values of the SUSY particle masses of the chosen benchmark point (*model II*) and estimated experimental statistical accuracies at CLIC [20]. All values are in GeV. The last column is either out of kinematic reach or not studied. One can find in Appendix C updated values of the statistical accuracies shown below.

Particle	Mass	Stat. acc.
$\tilde{\chi}_1^0$	340.3	± 4.0
$\tilde{\chi}_2^0$	643.1	± 13.0
$\tilde{\chi}_3^0$	905.5	± 19.0
$\tilde{\chi}_4^0$	916.7	± 20.0
$\tilde{\chi}_1^\pm$	643.2	± 7.0
$\tilde{\chi}_2^\pm$	916.7	± 7.0
$\tilde{e}_R^\pm$	1010.8	± 12.0
$\tilde{\mu}_R^\pm$	1010.8	± 14.4
$\tilde{\nu}_1$	1097.2	± 74.0

Particle	Mass	Stat. acc.
h	118.5	± 0.1
A	742.8	± 3.0
H	742.0	± 3.0
$H^\pm$	747.6	± 2.5

Quantity	Value	Stat. acc.
$\Gamma(A)$	21.7	± 3.5
$\Gamma(H^\pm)$	20.3	± 3.5

Particle	Mass
$\tilde{\tau}_1$	670
$\tilde{\tau}_2$	974
$\tilde{t}_1$	1393
$\tilde{t}_2$	1598
$\tilde{b}_1$	1544
$\tilde{b}_2$	1610
$\tilde{u}_R$	1818
$\tilde{u}_L$	1870
$\tilde{g}$	1812

Table 1.2: Fitted parameters in GeV from the chargino/neutralino sector. Each column represents a local minimum in the best fit to the data.

M_1	342.1 ± 4.1	-341.9 ± 4.1	341.9 ± 4.1	-342.2 ± 1.0
M_2	655.3 ± 6.5	655.3 ± 6.5	654.2 ± 6.5	654.2 ± 6.5
μ	924.8 ± 6.2	924.8 ± 6.2	-925.5 ± 6.2	-925.5 ± 6.2

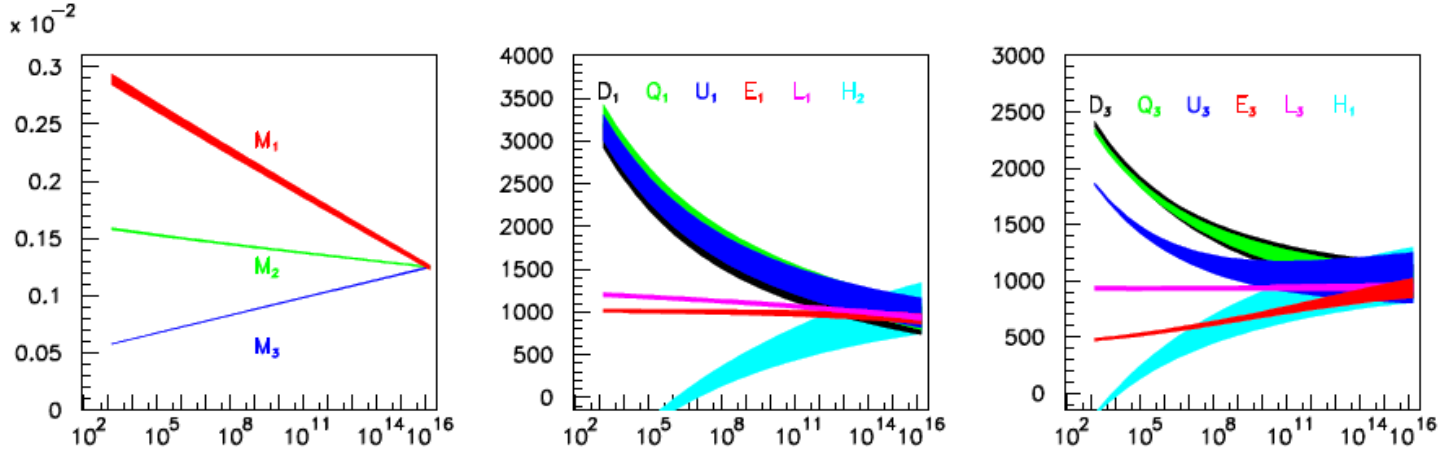

Fig. 1.10: Extrapolation of SUSY-breaking parameters from the electroweak to the GUT scale for *model II*, assuming 3% measurement precision on the physical sfermion masses. Axes units are GeV, except the vertical axis of the left-most panel which is in units of GeV^{-1}.

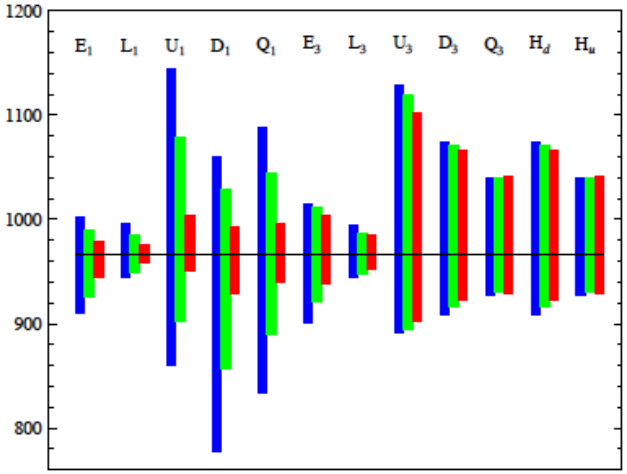

Fig. 1.11: One sigma range of the determined scalar mass parameters at the GUT scale assuming 5% (blue), 3% (green) and 1% (red) measurement precision on the physical sfermion masses. The black line indicates the nominal value $m_0 = 966$ GeV. Vertical axis is mass in units of GeV.

Table 1.3: Uncertainties on the SUSY breaking parameters at $Q = 1.5$ TeV for different expected precision on sfermion masses.

parameter	central value	accuracy (±)		
		$\Delta m/m$=0.05	$\Delta m/m$=0.03	$\Delta m/m$=0.01
M_1	345.2	4.0	3.9	2.9
M_2	631.8	6.4	6.4	6.3
M_3	1723	16	14	8
$M^2_{H_d}$	$-(435)^2$	$(109)^2$	$(109)^2$	$(109)^2$
$M^2_{H_u}$	$-(904)^2$	$(107)^2$	$(107)^2$	$(107)^2$
$M^2_{E_1}$	$(1008)^2$	$(157)^2$	$(157)^2$	$(156)^2$
$M^2_{L_1}$	$(1096)^2$	$(132)^2$	$(130)^2$	$(113)^2$
$M^2_{D_1}$	$(1760)^2$	$(480)^2$	$(378)^2$	$(227)^2$
$M^2_{U_1}$	$(1766)^2$	$(480)^2$	$(378)^2$	$(227)^2$
$M^2_{Q_1}$	$(1817)^2$	$(500)^2$	$(388)^2$	$(223)^2$
$M^2_{E_3}$	$(690)^2$	$(140)^2$	$(130)^2$	$(93)^2$
$M^2_{L_3}$	$(966)^2$	$(145)^2$	$(140)^2$	$(108)^2$
$M^2_{D_3}$	$(1547)^2$	$(209)^2$	$(200)^2$	$(154)^2$
$M^2_{U_3}$	$(1361)^2$	$(138)^2$	$(136)^2$	$(128)^2$
$M^2_{Q_3}$	$(1527)^2$	$(197)^2$	$(189)^2$	$(146)^2$
$\tan\beta$	51	3	3	3

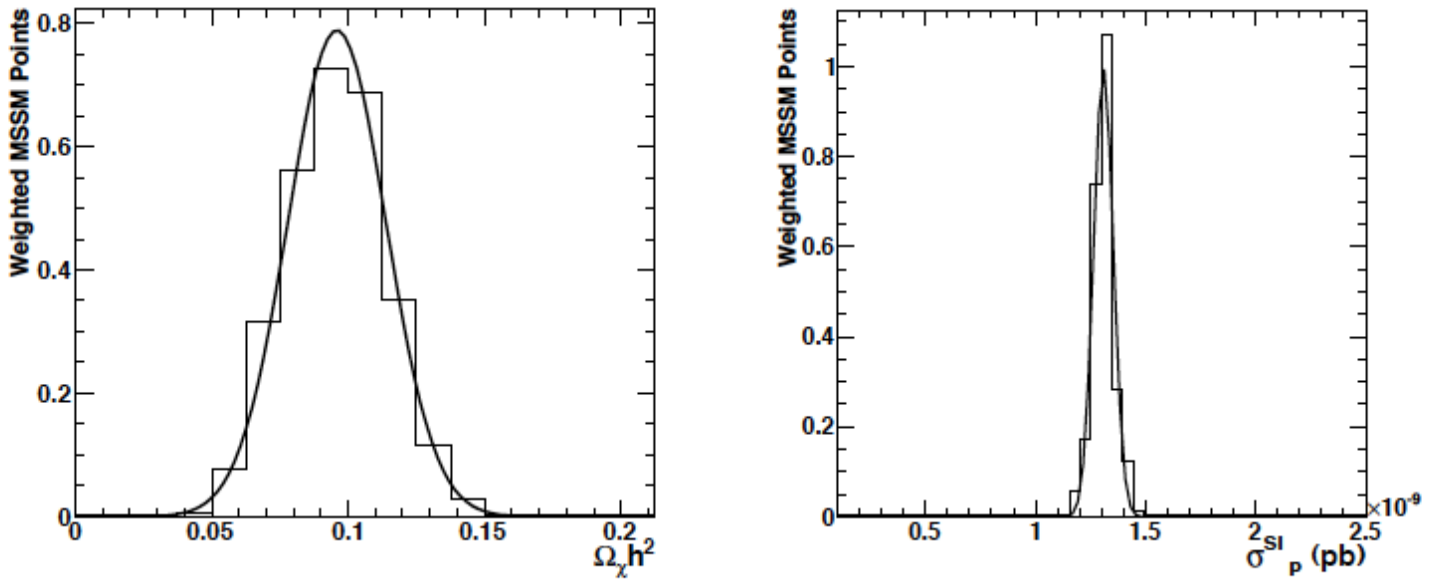

Fig. 1.12: Using probability weighted ensemble of scanned SUSY model points, the reconstructed neutralino relic density (left, using `SuperIsoRelic`) and predicted direct dark matter detection cross section (right, using `micrOMEGAs`) for the measurements of *model II*.

1.4 Higgs Strong Interaction

The couplings of a light scalar h to the SM vector bosons and to itself can be characterised in terms of the following Lagrangian (with $v \approx 246$ GeV) [59]

$$\mathscr{L} = \frac{1}{2}\left(\partial_\mu h\right)^2 - V(h) + \left(m_W^2 W_\mu^+ W^{\mu -} + \frac{m_Z^2}{2} Z_\mu Z^\mu\right)\left[1 + 2a\frac{h}{v} + b\frac{h^2}{v^2} + \dots\right] + \dots, \tag{1.1}$$

where $V(h)$ is the potential for h,

$$V(h) = \frac{1}{2} m_\mathrm{h}^2 h^2 + d_3\left(\frac{m_\mathrm{h}^2}{2v}\right) h^3 + d_4\left(\frac{m_\mathrm{h}^2}{8v^2}\right) h^4 + \dots, \tag{1.2}$$

and a, b, d_3, d_4 are arbitrary dimensionless parameters. The dots stand for terms of higher order in h. For the SM Higgs boson $a = b = d_3 = d_4 = 1$ and all the higher order terms vanish. The dilaton couplings are characterised by the relation $a = b^2$. The scattering amplitude of $V_L V_L \to \mathrm{hh}$ depends on a, b and d_3 and can be conveniently written as $\mathscr{A} = a^2\left(\mathscr{A}_{SM} + \mathscr{A}_1 \delta_b + \mathscr{A}_2 \delta_{d_3}\right)$, where $\mathscr{A}_{SM}$ is the value predicted by the SM and

$$\delta_b \equiv 1 - \frac{b}{a^2}, \qquad \delta_{d_3} \equiv 1 - \frac{d_3}{a}. \tag{1.3}$$

At large partonic centre-of-mass energies, $E \gg m_V$, $\mathscr{A}_1$ grows like E^2, while $\mathscr{A}_2$ (as well as $\mathscr{A}_{SM}$) is constant. The parameter δ_b thus controls the energy growth of the amplitude and gives a genuine "strong coupling" signature. On the contrary, δ_{d_3} determines the value of the cross section at threshold. In an $\mathrm{e^+e^-}$ collider the scattering $V_L V_L \to \mathrm{hh}$ can be studied via the process $\mathrm{e^+e^-} \to \nu\bar{\nu}\mathrm{hh}$, whose cross section can be written as

$$\sigma = a^4 \sigma_{SM}\left(1 + A\delta_b + B\delta_{d_3} + C\delta_b\delta_{d_3} + D\delta_b^2 + E\delta_{d_3}^2\right), \tag{1.4}$$

where σ_{SM} denotes its SM value. The energy behaviour of the underlying hard scattering is encoded in the coefficients A, B, C, D, E. By means of suitable kinematic cuts one can disentangle the high-energy behaviour from the physics at threshold, and extract δ_b, δ_{d_3} [61].

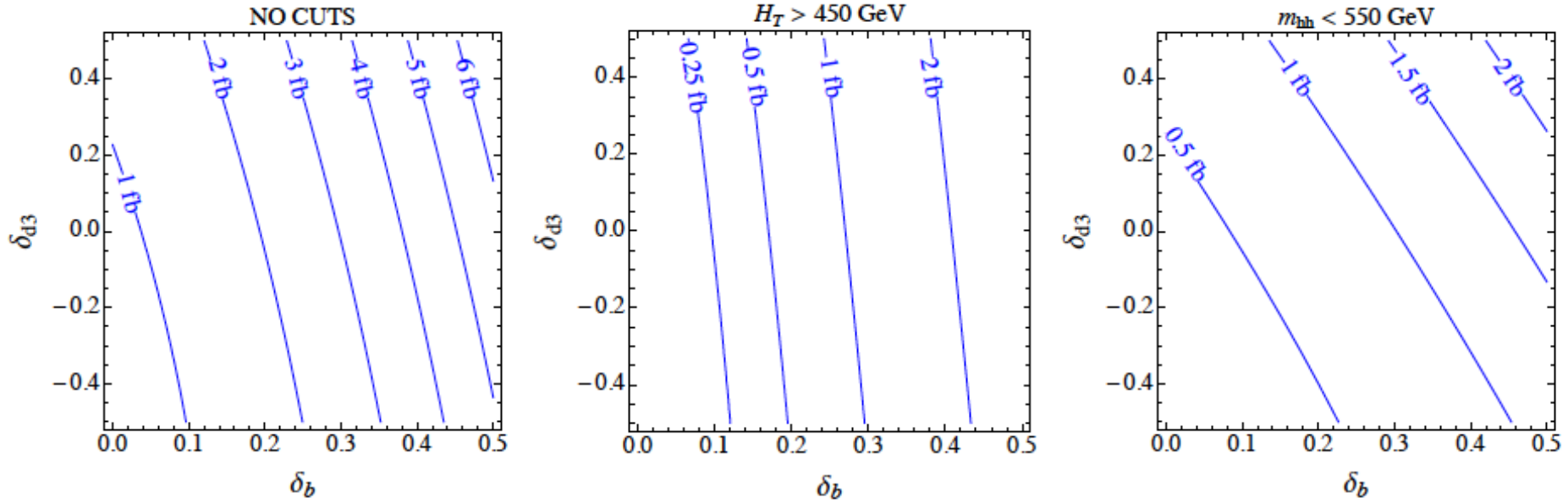

Fig. 1.13: Contours of constant cross section $\sigma(e^+e^- \to \nu\bar{\nu}hh)$ for $\sqrt{s} = 3$ TeV and $m_h = 120$ GeV in the plane (δ_b, δ_{d_3}). The three plots have been obtained by imposing no cuts (left), $H_T \geq 450$ GeV (centre), $m_{hh} < 550$ GeV (right) respectively.

Table 1.4: Statistical errors $(\Delta\delta_b, \Delta\delta_{d3})$ on the parameters δ_b and δ_{d_3} for $\sqrt{s} = 3$ TeV, $\mathscr{L} = 1\text{ab}^{-1}/a^4$ and $m_{\text{h}} = 120$ GeV. The value of the optimised cuts ranges in the interval $H_T^+ = 250 - 450$ GeV, $m_{\text{hh}}^- = 450 - 650$ GeV.

δ_b	δ_{d_3}					
	-0.5	-0.3	-0.1	0.1	0.3	0.5
0	(0.02,0.2)	(0.02,0.1)	(0.01,0.08)	(0.01,0.06)	(0.01,0.05)	(0.01,0.05)
0.01	(0.02,0.2)	(0.01,0.1)	(0.01,0.07)	(0.01,0.06)	(0.01,0.05)	(0.009,0.05)
0.02	(0.02,0.2)	(0.01,0.1)	(0.01,0.07)	(0.009,0.06)	(0.009,0.5)	(0.009,0.05)
0.03	(0.01,0.2)	(0.01,0.1)	(0.01,0.07)	(0.009,0.05)	(0.008,0.05)	(0.008,0.05)
0.05	(0.01,0.1)	(0.01,0.09)	(0.008,0.06)	(0.008,0.05)	(0.008,0.05)	(0.008,0.04)
0.1	(0.009,0.1)	(0.008,0.07)	(0.007,0.06)	(0.007,0.05)	(0.007,0.04)	(0.007,0.04)
0.2	(0.008,0.08)	(0.007,0.06)	(0.007,0.05)	(0.007,0.04)	(0.007,0.04)	(0.007,0.04)
0.3	(0.007,0.06)	(0.007,0.05)	(0.007,0.05)	(0.007,0.04)	(0.007,0.04)	(0.007,0.04)
0.4	(0.007,0.05)	(0.007,0.05)	(0.007,0.05)	(0.006,0.04)	(0.006,0.04)	(0.007,0.04)
0.5	(0.007,0.05)	(0.007,0.05)	(0.006,0.04)	(0.006,0.04)	(0.006,0.04)	(0.006,0.04)

Table 1.5: Statistical relative error $\Delta\xi/\xi$ for $\sqrt{s}$ =3 TeV with $\mathscr{L} = 1$ ab^{-1}. The value of the optimised cut $H_T \geq H_T^+$ ranges in the interval $H_T^+ = 300 - 500$ GeV. The numbers in parentheses report the relative error $\Delta\xi/\xi$ obtained without imposing any cut.

m_h	ξ					
[GeV]	0.01	0.03	0.05	0.1	0.2	0.3
120	1.1 (1.9)	0.3 (0.5)	0.1 (0.3)	0.06 (0.09)	0.03 (0.03)	0.02 (0.02)
150	1.1 (2.2)	0.3 (0.5)	0.2 (0.3)	0.06 (0.09)	0.03 (0.03)	0.02 (0.02)
180	1.2 (2.7)	0.3 (0.6)	0.2 (0.3)	0.07 (0.09)	0.03 (0.03)	0.02 (0.02)

$\xi = (v/f)^2$ and f is the decay constant of the pseudo-NG Higgs boson.

1.5 Z', Contact Interactions and Extra Dimensions

$$\mathscr{L}_{CI} = \sum_{i,j=L,R} \eta_{ij} \frac{g^2}{\Lambda^2} (\bar{e}_i \gamma^\mu e_i)(\bar{f}_j \gamma_\mu f_j)$$

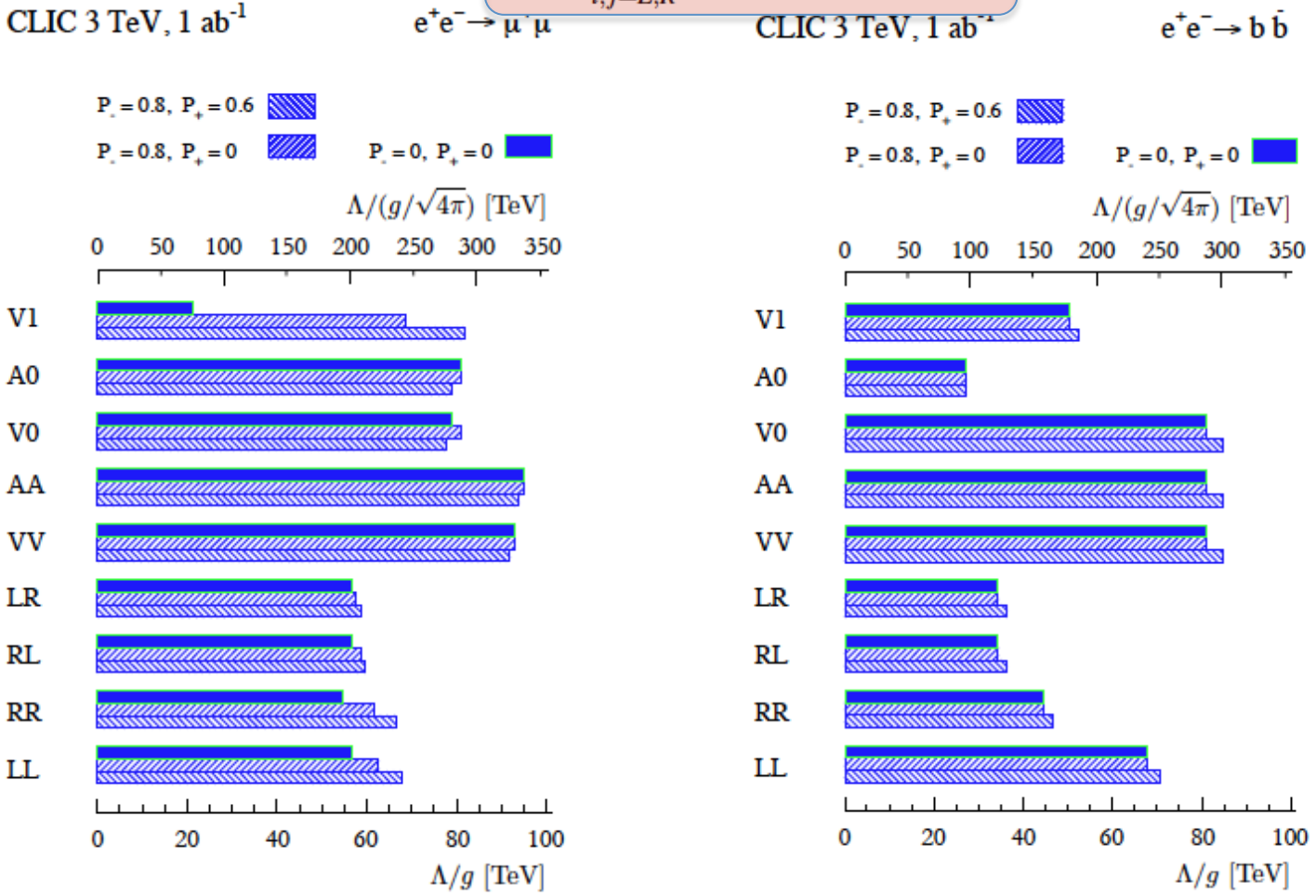

Fig. 1.14: Limits on the scale of contact interactions (Λ/g) that can be set by CLIC in the $\mu^+\mu^-$ (left) and $b\bar{b}$ (right) channels with $\sqrt{s} = 3$ TeV and $\mathscr{L} = 1$ ab^{-1}. A degree of polarisation $P_- = 0, 0.8$ $(P_+ = 0, 0.6)$ has been assumed for the electrons (positrons). The various models are defined in Table 6.6 of [20], except the model V1 which is defined as $\{\eta_{LL} = \pm, \eta_{RR} = \mp, \eta_{LR} = 0, \eta_{RL} = 0\}$.

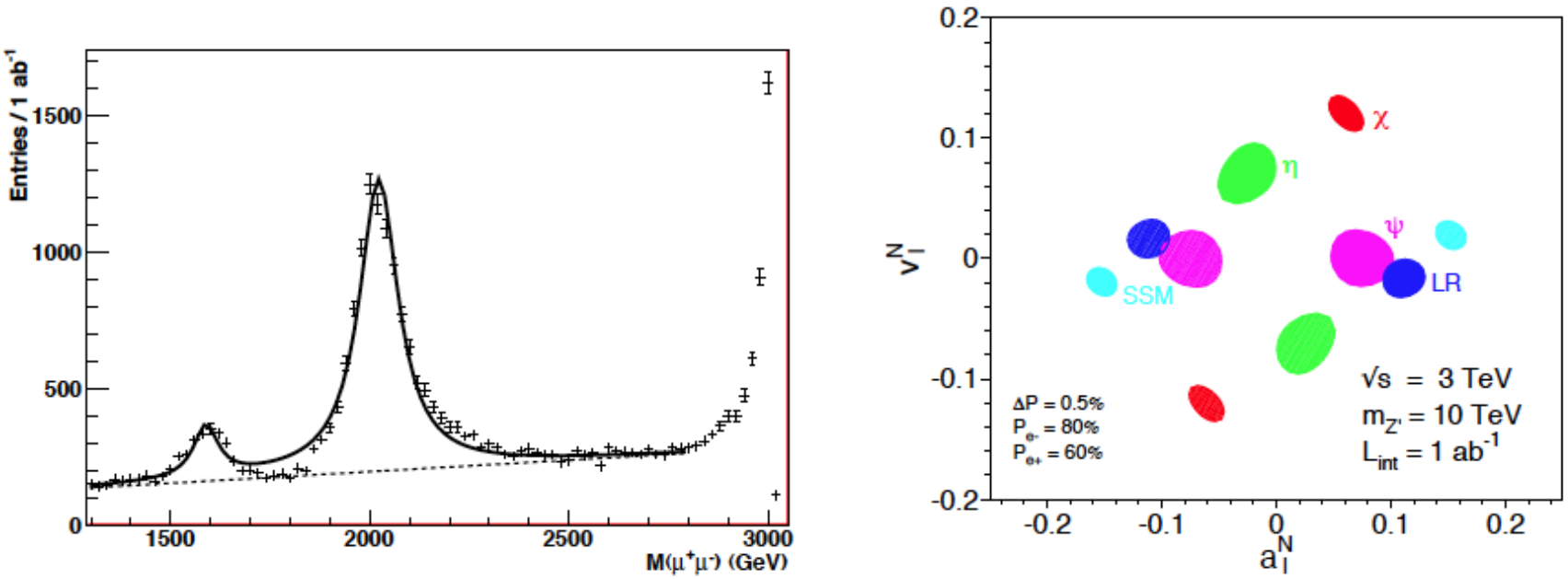

Fig. 1.15: Left: Observation of new gauge boson resonances in the $\mu^+\mu^-$ channel by auto-scan at 3 TeV. The two resonances are the $Z_{1,2}$ predicted by the 4-site Higgsless model of [64]. Right : Expected resolution at CLIC with $\sqrt{s} = 3$ TeV and $\mathscr{L} = 1$ ab^{-1} on the "normalised" leptonic couplings of a 10 TeV Z′ in various models, assuming lepton universality. The couplings can be determined up to a twofold ambiguity. The mass of the Z′ is assumed to be unknown. χ, η, ϕ refer to various linear combinations of $U(1)$ subgroups of E_6; the SSM has the same couplings as the SM Z; and, LR is $U(1)$ surviving in Left-Right model. The two fold ambiguity is due to the inability to distinguish (a, v) from $(-a, -v)$.

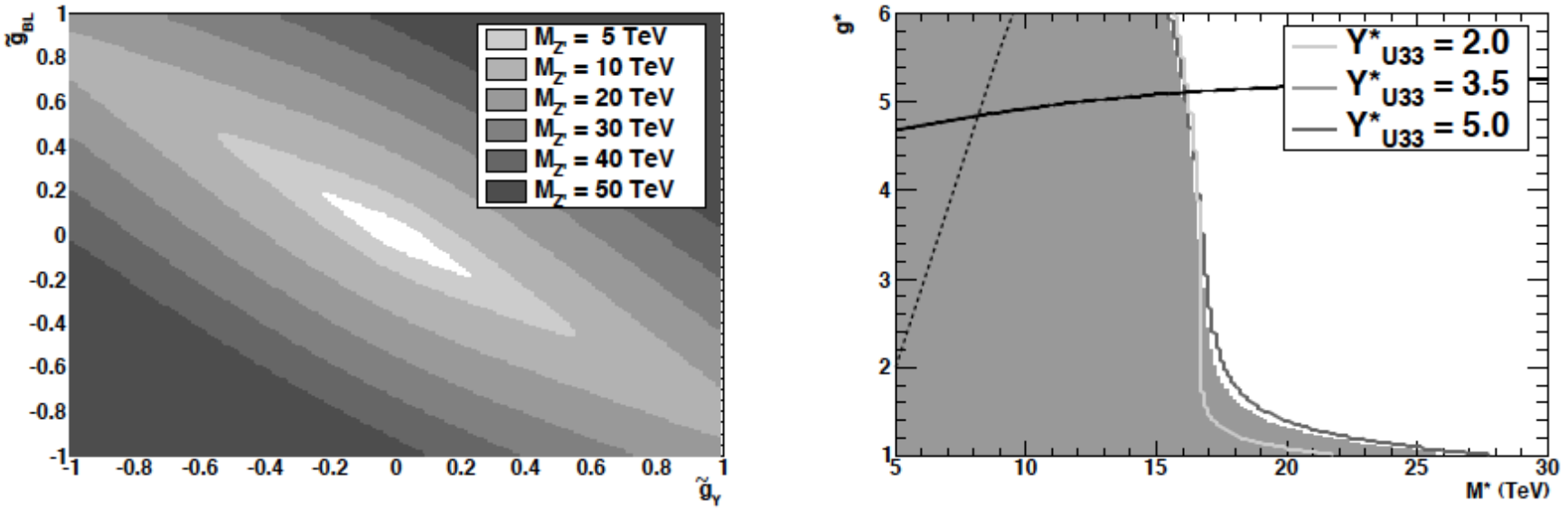

Fig. 1.16: Left: Sensitivity to the Z' minimal model in the $\tilde{g}_{BL}$ vs. $\tilde{g}_Y$ plane for various values of $M_{Z'}$. Right: Sensitivity to the warped/composite two-site model in the (M_*, g_*) plane for different values of Y_{*U33}. The region above the continuous line has the broader resonance with $\Gamma > 0.5\ M$ and our perturbative calculations cannot be trusted. The region above the dashed line is excluded by present electroweak data for $Y_{*U33} = 2$ but is allowed for larger values of Y_{*U33}. In both plots we assume $\sqrt{s} =$ 3 TeV with 2 ab^{-1} of luminosity and polarised beams (80% for electrons and 60% for positrons).

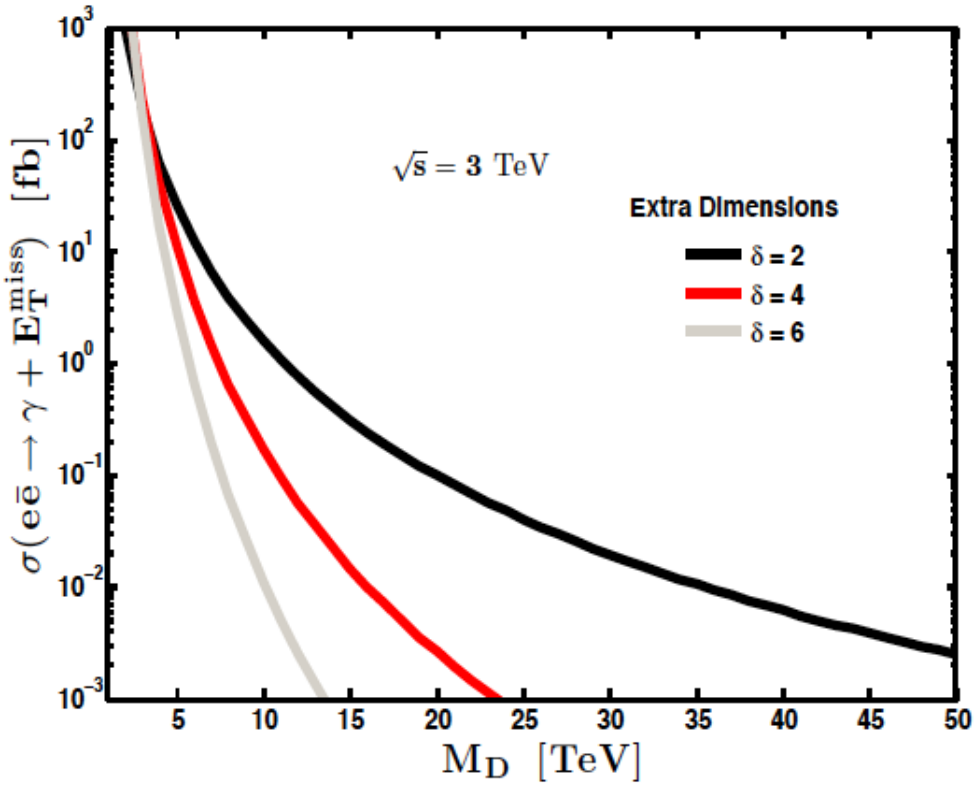

Fig. 1.17: Cross section of photon plus missing energy for ADD flat extra dimensions scenario as a function of the fundamental gravity mass scale M_D. Lines are drawn for $\delta = 2,4,6$ extra dimensions. The SM background is approximately 23 fb, which implies sensitivities to M_D of at least 14, 9 and 6 TeV for $\delta = 2,4,6$ respectively with over 1 ab^{-1} accumulated.

1.7 Discussion and Conclusions

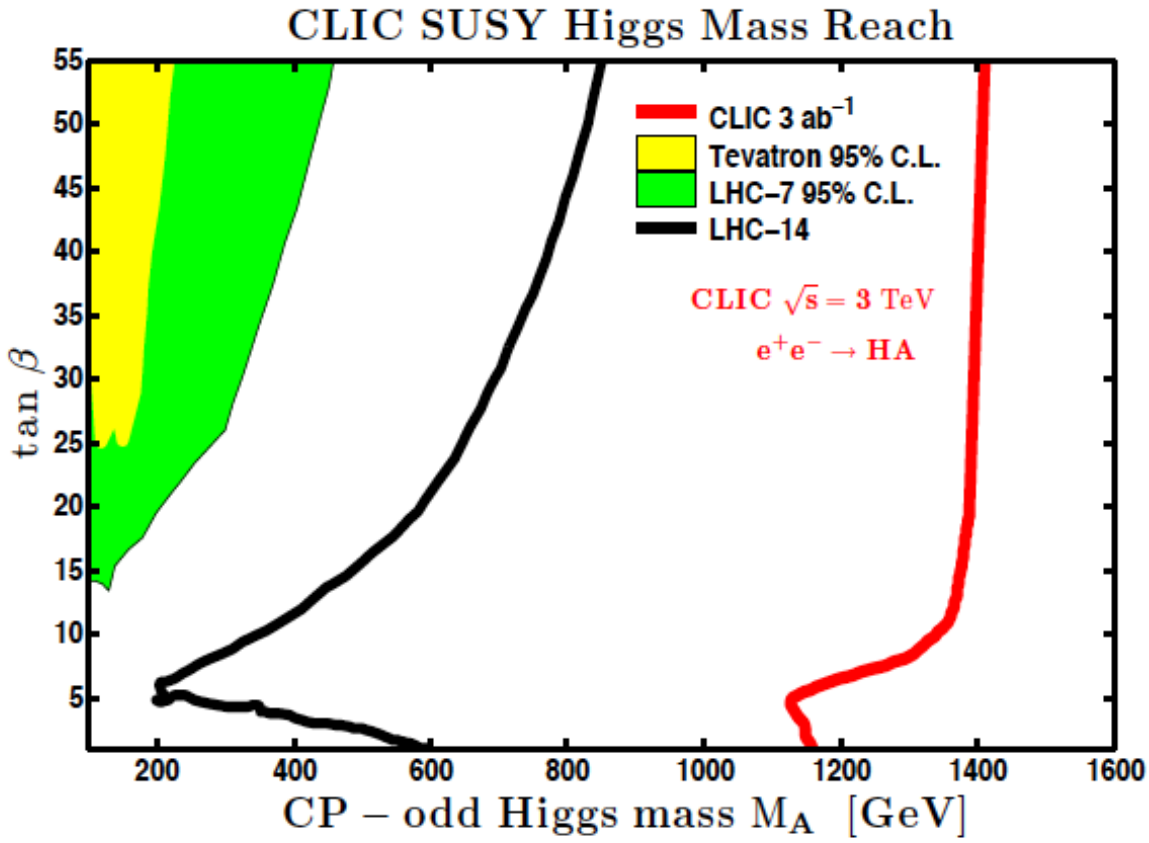

Fig. 1.18: Search reach in the $m_A - \tan\beta$ plane for LHC and CLIC. The left-most coloured regions are current limits from the Tevatron with ~ 7.5 fb^{-1} of data at $\sqrt{s} = 1.96$ TeV and from ~ 1 fb^{-1} of LHC data at $\sqrt{s} = 7$ TeV. The black line is projection of search reach at LHC with $\sqrt{s} = 14$ TeV and 300 fb^{-1} of luminosity [78]. The right-most red line is search reach of CLIC in the HA mode with $\sqrt{s} = 3$ TeV. This search capacity extends well beyond the LHC. A linear collider at $\sqrt{s} = 500$ GeV can find heavy Higgs mass eigenstates if their masses are below kinematic threshold of 250 GeV.

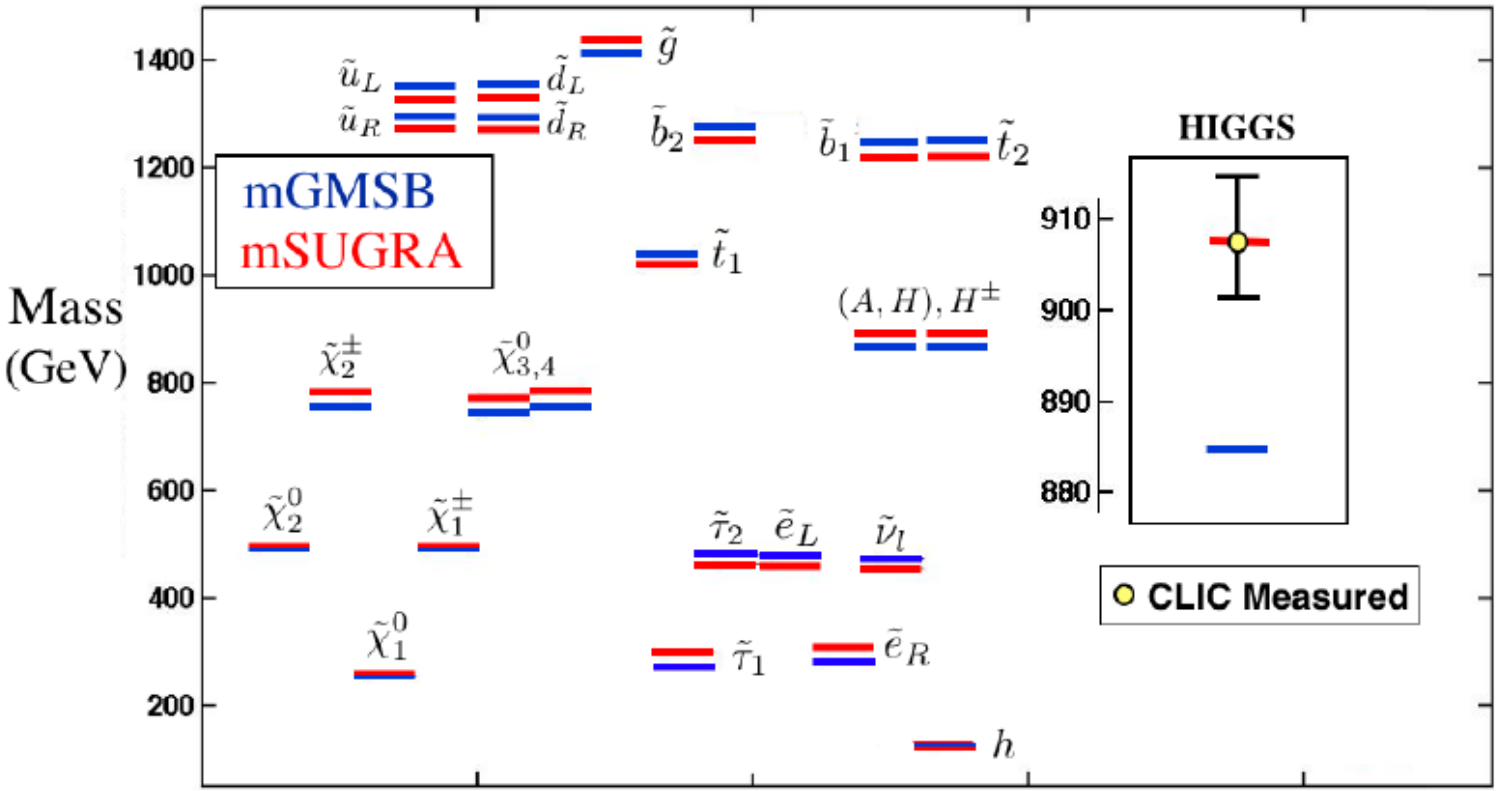

Fig. 1.19: Resolving SUSY breaking models and masses with CLIC: Shown are the nearly degenerate spectra of a mSUGRA model and a mGMSB model. Assuming some of the SUSY particles masses are measured, with a spectrum of the type above predicted by the different models of Supersymmetry breaking, CLIC would be able to discern not only some of the slepton masses and the heavier charginos within the two models, but also the SUSY Higgs masses. For mSUGRA the soft masses are $m_0 = 175$ GeV, $m_{1/2} = 645$ GeV, $A_0 = 0$, with $\tan\beta = 10$ and $\mu > 0$. For mGMSB the number of messengers are $n_l = n_q = 5$, and $\Lambda_{\rm SUSY} = 4 \cdot 10^4$ GeV, $M_{\rm Mess} = 10^{12}$ GeV, with $\tan\beta = 10$.

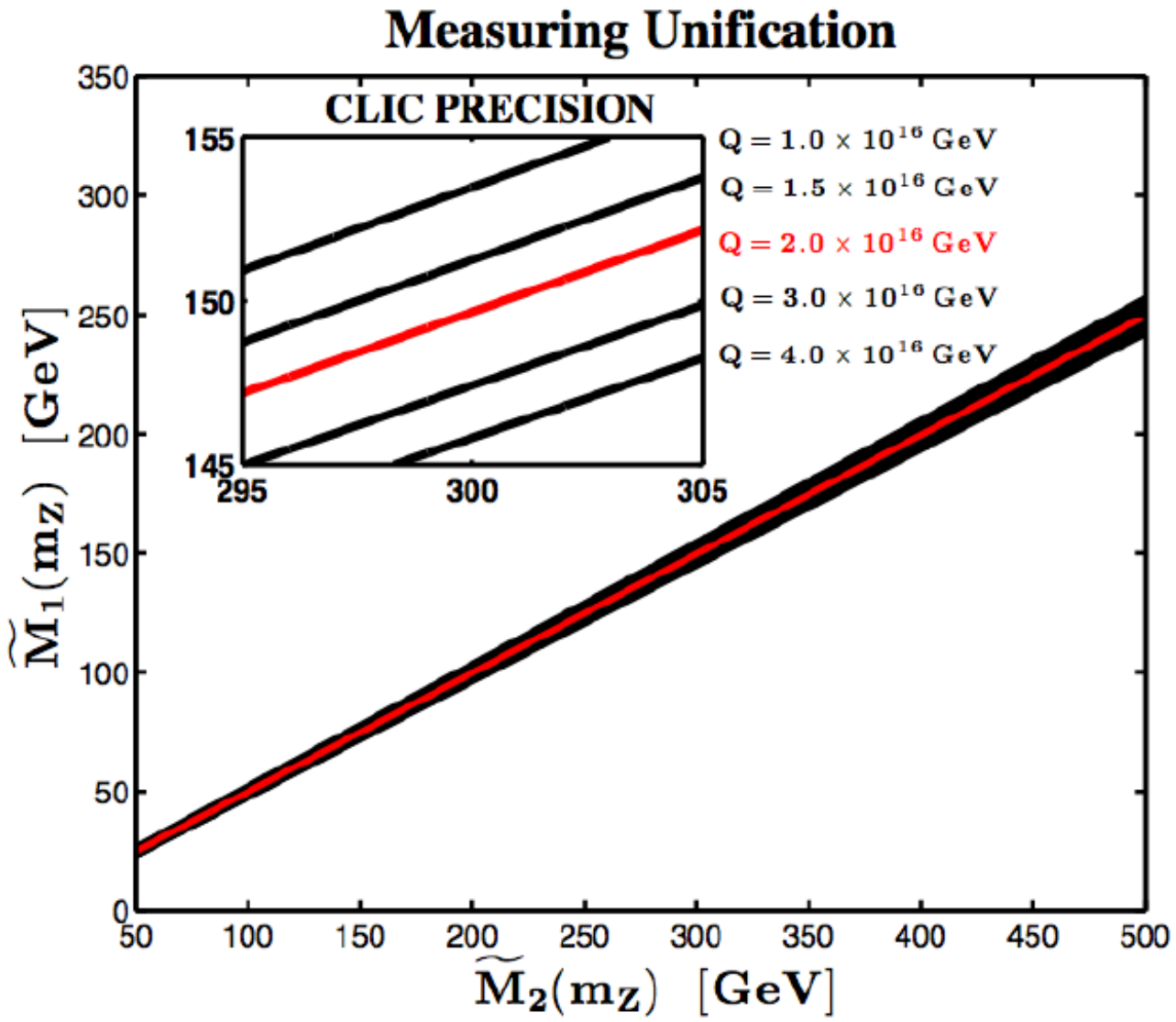

Fig. 1.20: M_2 vs. M_1 at the low scale assuming unification of the gauginos at various high-energy scales Q, which can test compatibility with the scale of gauge coupling unification at $Q \simeq 2 \cdot 10^{16}$ GeV. The precision on the gaugino masses are represented by the full range of the inset box.

Table 1.6: Discovery reach of various theory models for different colliders [70]. LHC14 is defined to be the LHC at $\sqrt{s}$ =14 TeV with 100 fb^{-1} of integrated luminosity, while SLHC is with 1 ab^{-1}. LC800 is a 800 GeV e^+e^- collider with 500 fb^{-1}, and CLIC3 is $\sqrt{s}$ =3 TeV with 1 ab^{-1}. TGC is short for Triple Gauge Coupling, and "μ contact scale" is short for LL μ contact interaction scale Λ with $g = 1$ (see Section 1.4).

New particle	LHC14	SLHC	LC800	CLIC3
squarks [TeV]	2.5	3	0.4	1.5
sleptons [TeV]	0.3	-	0.4	1.5
Z' (SM couplings) [TeV]	5	7	8	20
2 extra dims M_D [TeV]	9	12	5-8.5	20-30
TGC (95%) (λ_γ coupling)	0.001	0.0006	0.0004	0.0001
μ contact scale [TeV]	15	-	20	60
Higgs compos. scale [TeV]	5-7	9-12	30	30

‘Internal Review’

Members of community asked to communicate their reviews and critiques of the Physics Potential chapter.

Comments by others and views of Gian and myself have been collected.

These ‘chapter 1 internal reviews’ under discussion now.

Finally, lots of good work by many people. The overall physics case looks strong.